

H.R. DASHTOYAN

**MICROWAVE (RF) SIGNAL GENERATION  
ON THE METAL-FERROELECTRIC-METAL NANOSTRUCTURE**

Microwave (dynamic) characteristics of barrier-injected transit-time metal-ferroelectric-metal nanostructure are investigated for the first time. It is shown that: it is possible to obtain dynamic negative resistance and therefore the microwave signal generation (amplification) on such structures; the power output and efficiency increase with an increase of the concentration of oxygen vacancies conditioned traps in ferro-films; based on the obtained results, and combining them with the passive elements already used based on ferro-thin films, one can construct fully integrated Ferro-VLSI circuits.

**Keywords:** metal-ferroelectric-metal nanostructure, dynamic characteristics, Ferro-VLSI circuit.

**Introduction.** The perovskite oxides  $A_{1-x}A'_xB O_{3-b}$  ( $A=Pb, Ba, La, Li; A'=Sr, Ca; B=Ti, Ta, Co, Fe$ , etc.) have been used in many applications due to their large nonlinear optical coefficients, large dielectric constants, thermal stability and higher catalytic properties. These include high density DRAMs, non-volatile FeRAMs, ferroelectric FETs, SOFCs, voltage-tunable capacitors, microwave electronic components that can work especially at GHz [1-6]. These devices are a novel class of solid-state devices and are expected to be very promising for applications in information storage, surface acoustic wave resonators and tunable varactors, bio(chemical) sensors, transducers and actuators (including ultrasonic, infrared and imaginary applications), micromechanical systems (MEMS), optoelectronics, and have a large potential for new multifunctional device applications. Moreover, by using these advantageous properties of perovskite oxides, a number of advanced high-frequency tunable capacitors have been successfully demonstrated and integrated into RF components, such as phase shifters and RF filters [2-5]. Due to the presence of oxygen vacancies and ionic conductance, perovskite oxides have a high catalytic activity in oxygen reduction and oxidation, and thus suitable for a large variety of sensor applications [7-10].

While these devices' ferroelectric, pyroelectric, piezoelectric, microwave and electro-optic properties have been well studied experimentally, very little is known about the possibilities of generation (amplification) of microwave (RF) signals on ferroelectric-based structures. In this connection, if we have generation (amplification) of signals on ferroelectric-based devices, one can speak about fully integrated Ferro-VLSI circuits.

The goal of this work is to investigate the possibilities of microwave (RF) signal generation (amplification) on the metal-ferroelectric-metal (m-f-m) nanostructure for the first time. Our previous theoretical calculations have shown that in such a structure, at microwave (RF) frequencies, it is possible to obtain signal generation.

**Theory.** As it is well known [11-15], the dynamic negative resistance (DNR) effects can increase in transit-time semiconductor devices (IMPATT, TUNNETT, BARITT) if the phase lag of the modulation component of the current, which is in anti-phase with the local electric field, is increased. To achieve such conditions, that is for an increase of the DNR (therefore increase of the output power), it is necessary to have drift region materials:

- a) with low charge carrier mobility;
- b) with higher resistivity;
- c) to have injection contacts;
- d) to operate the drift region punch-through regime.

For this reason, the use of ferroelectrics is promising also owing to the fact that the charge mobility in the ferroelectrics is rather small, which leads to an increase in the phase delay between the current and alternating electric field in the microwave range and, hence, to an increase in the absolute magnitude of DNR. The use of *ferroelectrics as a drift region material* is promising because the magnitude of electrical breakdown voltage in ferroelectrics is higher in comparison with other semiconductor materials. Here we expect an increase in the amplitude of the microwave signal, all other factors being equal.

In our previous calculations and estimations, it has been shown that all these requirements are easy and possible to achieve in *m-f-m* structures.

Moreover, our theoretical calculations, carried out for m-f-m structures, are based on the assumptions that:

- a) in a metal-ferroelectric contact, the presence of high concentration of oxygen vacancies (as the most mobile and abundant defects in perovskite oxides) is “endowed” ferroelectric to n-type semiconductor properties and the ferroelectric core exhibits p-type semiconductor properties [1-6,16,17];
- b) point defects (i.e. oxygen vacancies) create energy levels for charge carriers in the gap of ferroelectrics: deep-level trapping states with energies in the range of  $E_v+2.4eV$  to  $E_v+3.15eV$  and a series of shallower traps near the conduction band edge in the range of  $E_c - E_t=0.06...0.4 eV$ . These electron traps are attributed to oxygen vacancy or ion transition-metal/oxygen vacancy defects. The point charge concentration ranges from  $10^{16}$  to  $10^{20} cm^{-3}$  in the as-grown films [1-6, 16,17];
- c) the dielectric permittivity of ferroelectric materials is in nonlinear dependence on the applied electric field:  $\varepsilon(E, r) = \varepsilon(0)(1 + AE^2)^{-1}$ , where  $A = 3\beta[\varepsilon_0\varepsilon(0)]^3$ , and  $\varepsilon(0)$  is the permittivity at the zero bias. For example, for SrTiO<sub>3</sub>,  $\beta= 8\cdot 10^9 V\cdot m^5/C^3$ ,  $\varepsilon(0) = 300$  and  $A=0.45\cdot 10^{-15} (m/V)^2$  [1-6];

d) under an applied DC field, the traps release electrons via Poole-Frenkel mechanism and become charged. This oxygen vacancies - “conditioned” charge leads to a change in the trapped electron occupation function, and due to this, a new high localized field, polarized inclusions are formed in films. The electric field of a point charge polarizes the crystal, locally reducing its permittivity which, in turn, can bring to hysteresis behaviour in  $C(V)$  and dielectric constant,  $\varepsilon(V)$ , as well as can have. An influence on the  $I(V)$  dependence and other polarization processes [18-20].

Based on these assumptions, using the theory of transit-time devices [11-15] for the m-f-m structure punch-through ( $V_{Rt}$ ) and flat band ( $V_{FB}$ ) voltages are received:

$$V_{Rt} = \left\{ \frac{4\varepsilon_r^2}{q^2 N_t^2 A} \left[ \frac{l}{\sqrt{A}} + \left( \frac{2qN_t V_{bi}}{\varepsilon_r} \right)^{1/2} \right]^2 - \frac{l^2}{A} \right\}^{1/2},$$

$$V_{FB} \cong \frac{\varepsilon_r}{qN_t A} \left[ 1 + \sqrt{1 - \frac{l^2 q N_t A}{\varepsilon_r^2}} \right] \cong \frac{\varepsilon_r}{qN_t A},$$

where  $\varepsilon_r = \varepsilon_0 \varepsilon(0)$ ;  $l$  is the length of ferro-film;  $N_t$  is the concentration of oxygen vacancies near the metal-ferroelectric contacts,  $q$  is the electronic charge;  $V_{bi}$  is the built-in potential in the ferro-film metal contact.

The small signal impedance of the examined structure is presented as:

$$Z = -\frac{V_{1m}}{I_1} = R + jX, \quad (1)$$

where  $V_{1m}$  and  $I_1$  are the amplitude of the AC voltage and current respectively.

For a simple analysis and modeling of generation in the examined structure, two regimes of operation are studied, namely:

- a) high conductance injection regime (SCL injection:  $R_{SCL}$ );
- b) when the conductance of the injected contact is limited and controlled by a potential barrier (barrier-limited injection regime:  $R_{BL}$ ).

For the active component of impedance, the following expressions are obtained:

$$R_{BL} = R_{SCL1} + R_{B1}, \quad (2)$$

$$R_{SCL1} = \frac{\beta^2 \mu I_0 T^3}{\varepsilon \varepsilon_r^2 \theta^2 (\theta^2 + \theta_1^2)} \left\{ a_5 \left[ 1 + \frac{\varepsilon_r^2 \theta_t^2}{(\sigma \beta T)^2 + \theta^2 \varepsilon_r^2} \right] \right\} + \frac{a_6}{\theta^2 + \theta_1^2} + \frac{a_7 (\theta^2 + \theta_1^2)}{\theta^2 + \theta_2^2},$$

$$R_{B1} = \frac{\beta \theta_{0s} T^2}{\varepsilon_r \theta_t (\theta^2 + \theta_1^2)} \left\{ a_5 + \frac{a_7 (\theta^2 + \theta_1^2)}{\theta^2 + \theta_2^2} + \frac{a_8 \theta \theta_t \varepsilon_r^2}{[(\sigma \beta T)^2 + \theta^2 \varepsilon_r^2]} \right\}, \quad (3)$$

where  $\theta_2 = \theta_1 - \theta_t$ ,  $a_5 = \theta_1 - e^{\theta_1} (\theta \sin \theta + \theta_1 \cos \theta)$ ,  $a_7 = \theta \sin \theta - \theta_t \cos \theta + \theta_t e^{\theta_t}$ ,  $a_8 = e^{\theta_1} (\theta_1 \sin \theta - \theta \cos \theta)$ ,  $\beta = 1 + AE_0^2$ ,  $E_0$  is the DC electric field,  $\beta_1 = (n_0 + n_{t0})$ ,  $S$  - the cross section area of the ferro-film,  $\beta_2 = 2qAE_0$ ,  $\omega = 2\pi f$  - the signal angular

frequency,  $\vartheta_{0S}$  - the velocity of carriers at the injected metal-ferroelectric contact,  $\theta = \omega T$  - the transit angle,  $T$  is the transit time,  $\theta_t = \omega_t T$ ,  $\omega_t = \frac{qn_{t0}\mu\beta}{\varepsilon_r}$ ,  $n_{t0}$  - the equilibrium charge in traps,  $n_{t0} = \frac{n_0 N_t}{n_0 + \gamma}$ ,  $\gamma = \frac{N_C}{g} \exp\left(-\frac{E_t - F}{kT_r}\right)$ ,  $k$  - the Boltzmann's constant,  $T_r$  - the absolute temperature,  $N_C$  - the density of states in the ferro-film conductance band,  $g$  - the degeneracy factor,  $n_0$  - the free electron concentration,  $E_t \cong 0.06 \dots 0.4$  eV - the energy depth of oxygen vacancy-associated trap levels from the conductance band age of ferroelectric,  $\mu$  - the mobility of charge carriers in drift region,  $I_0$  - the density of DC,

$$\theta_1 = \frac{\beta_1 \beta_2 \mu I_0 T^2 \beta}{\varepsilon_r^2 \theta_t^2} (e^{\theta_t} - \theta_t - 1) + \frac{\beta_1 \beta_2 \vartheta_{0S} T}{\varepsilon_r \theta_t} (e^{\theta_t} - 1),$$

where  $\theta_1 = \omega_1 T$ ,  $\omega_1 = \frac{qN_t\mu\beta}{\varepsilon_r}$ ,  $\sigma \cong \frac{\mu I_0}{V_{0S}}$  is the conductance of the injected contact.

The analysis of expression (3) showed that the negative magnitude of  $R$  at the low levels of the charge carrier injection from the metal contact can appear over the range of such transit angles where the following inequality is fulfilled:

$$\cos \theta - \left( \frac{\theta_M \theta_T + \theta^2}{\theta_M \theta - \theta \theta_T} \right) \sin \theta > \exp(-\theta_M).$$

The corresponding angle range is approximately  $3.6 < \theta < 7.2$  with the optimum magnitude  $\theta_{op} \approx 1.5\pi$  for the maximal value of DNR. When  $\theta_{op} \approx 1.5\pi$ , the frequency is given by the formula  $f_0 \approx \frac{3V_S}{4L_d}$ . For example, if  $f = 100$  GHz,  $L_d \sim 1.5$   $\mu m$ , if  $f = 300$  GHz,  $L_d \sim 0.5$   $\mu m$ , and if  $f = 1000$  GHz,  $L_d \sim 1500$   $\text{Å}$ , respectively. As it is expected for transit-time devices, there is a specific length of the drift region  $L_d$ , which yields the maximal DNR for any given frequency, injected contact conductance, and saturation velocity.

The numerical estimates have been carried out for the parameters:  $\mu_1 \cong 0.1 \dots 3$   $cm^2/V_S$ ,  $I_0 = 10^2 \dots 10^3$   $A/cm^2$ ,  $S = 6 \cdot 10^{-8}$   $cm^2$ ,  $T \approx 10^{-11}$  s,  $\theta_0 = \frac{0.037\mu_1 I_{01}\beta}{V_{0S1}}$ ,  $V_{0S} \approx 10^4 \dots 10^5$   $cm/s$ ,  $\theta_t \cong 0.67 \cdot 10^{-5} \dots 3$ .

As it follows from the figures, with the increase of the traps' concentration (i.e. oxygen vacancies' concentration,  $N_t$ ), the DNR is increased in absolute value (Fig.1), but the frequency band, where it take place, becomes larger and displaced to a lower frequency (Fig. 2).

$$R = R_{SCL1} + R_{B1}, \text{ Ohm}$$

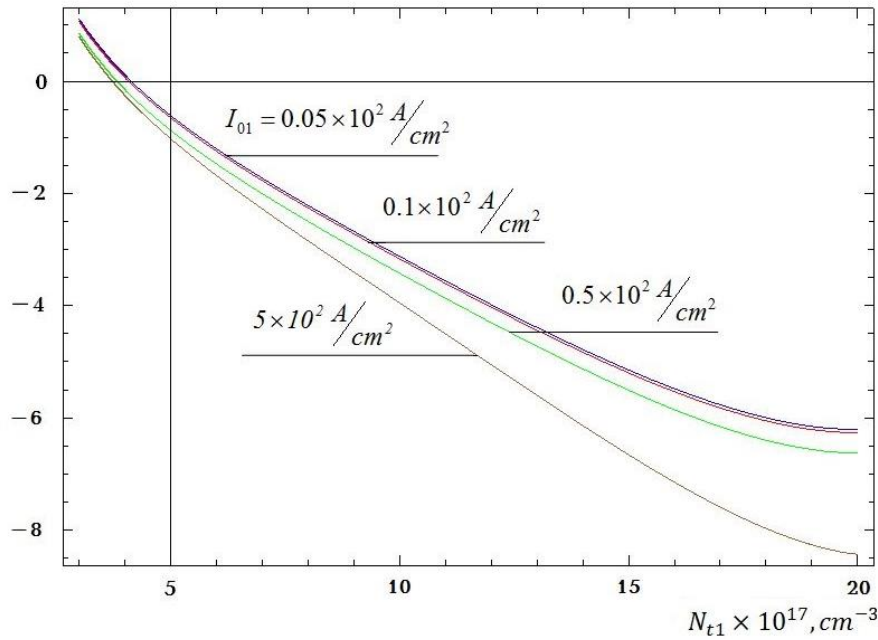


Fig. 1. Dependence of  $R_{SCL1}$ ,  $R_{B1}$ ,  $R = R_{SCL1} + R_{B1}$  (Ohm) on trap concentration  $N_{t1}$  ( $\times 10^{16} \text{ cm}^{-3}$ ) for the different values of  $I_{01}$  ( $\times 10^2 \text{ A/cm}^2$ ). The other parameters are:  $\beta=2.5$ ;  $\mu_1=1 \text{ cm}^2/\text{V}\cdot\text{s}$ ;  $E_{01}=3 \cdot 10^5 \text{ V/cm}$ ;  $V_{0S1}=5 \cdot 10^4 \text{ cm/s}$ ; area  $S=6 \cdot 10^{-8} \text{ cm}^2$ ; transit-time angle  $\theta=4$

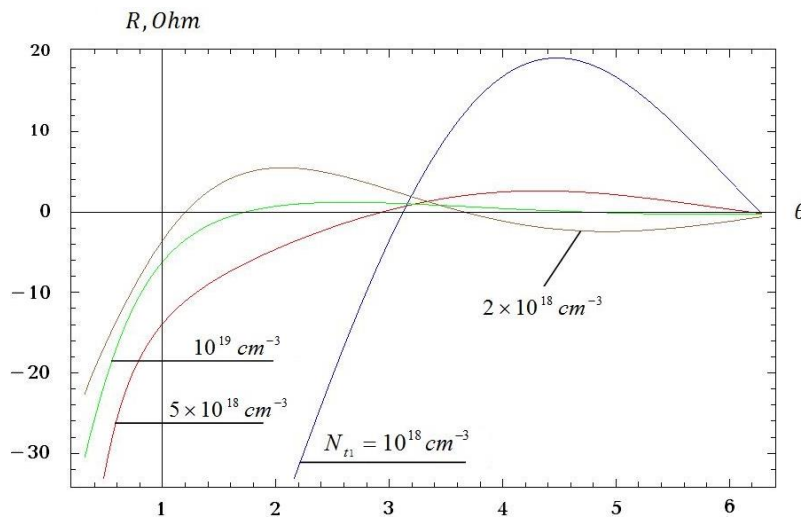


Fig. 2. Dependence of  $R_{SCL}$ ,  $R_B$ ,  $R = R_{SCL} + R_B$  (Ohm) on transit-time angle  $\theta$  for the different values of trap concentration  $N_{t1}$  ( $\times 10^{16} \text{ cm}^{-3}$ ). The other parameters are:  $\beta=1.7$ ;  $\mu=1 \text{ cm}^2/\text{V}\cdot\text{s}$ ;  $E_0=3 \cdot 10^5 \text{ V/cm}$ ;  $I_{01}=5 \cdot 10^2 \text{ A/cm}^2$ ;  $V_{0S}=5 \cdot 10^4 \text{ cm/s}$ ; area  $S=6 \cdot 10^{-8} \text{ cm}^2$

**Conclusions.** From the scientific and practical points of view, we anticipate that the new knowledge that emerges from this work will provide a basis for the development of a new class of ferroelectric nano-film-based active devices and integration of these devices with the ferro-passive elements used today to create for the future Very Large Scale Ferro-integrated Circuits (VLSFC). As it follows from figures 1 and 2, in m-f-m nanostructures, for certain materials and external applied signal conditions, it is possible to obtain generation (amplification) of the microwave signal and thus to construct fully integrated Ferro-VLSI circuits.

#### REFERENCES

1. **Dawber M., Raba J.F., Scott J.F.** Physics of thin-film ferroelectric oxides // Rev. of Modern Phys.– 2005.– Vol. 77.– P. 1083–1130.
2. **Gevorgian S.Sh., Tagantsev A.K., Vorobiev A.K.** Tunable Film Bulk Acoustic Wave Resonators.– London: Springer-Verlag, 2013.– 243 p.
3. Ferroelectric Materials for Microwave Tunable applications / **A.K. Tagantsev, V.O. Sherman, K.F. Astafiev, et al** // J. of Electroceramics.– 2003.– P. 11–66.
4. **Ishiwara H., Okuyama M. and Arimoto Y.(Eds.)**. Ferroelectric Random Access Memories: Fundamentals and Applications // Topics in applied physics.– 2004.– Vol. 93.– P. 165–176.
5. **Chen C.-Y., Chou J.-Ch., Chou H.-T.** pH Sensing of Ba<sub>0.7</sub>Sr<sub>0.3</sub>TiO<sub>3</sub>XSiO<sub>2</sub> Film for Metal-Oxide-Semiconductor and Ion-Sensitive Field-Effect Transistor Devices // Journal of the Electrochemical Society.– 2009.– 156, N6.– P. G59-G64.
6. Metal-ferroelectric-metal structures with Schottky contacts. Analysis of the experimental current-voltage and capacitance-voltage characteristics of Pb(Zn,Ti)O<sub>3</sub> thin films / **L. Pintilie, I. Boerasu, M.J.M. Gomes, et al** // J. Appl. Phys.- 2005.- Vol. 98.- P. 124104–124104.
7. **Agarwal S., Samanta S.B., Shara G.L.** Influence of pH on structural and electrical properties of sol-gel derived (Ba,Sr)TiO<sub>3</sub> thin films under humid conditions // Thin Solid Films.– 2004.– Vol. 48.– P. 502-508.
8. pH-sensitive properties of barium strontium titanate (BST) thin films prepared by pulsed laser deposition technique / **V.V. Buniatyan, M.H. Abouzar, N.W. Martirosyan, et al** // Phys. Status Solidi.- 2010.- A 207, N4.- P. 824-830.
9. Multi-parameter sensing using high-*k* oxide of barium strontium titanate / **C. Huck, A. Poghossian, M. Backer, et al** // Phys. Status Solidi.– 2015.– A212, N6.– P. 1254-1250.
10. **Wang J., Zhang T., Wan N., Xiang J.** Microstructure, dielectric and photoluminescence properties of Tm-doped Ba<sub>0.8</sub>Sr<sub>0.2</sub>TiO<sub>3</sub> thin films fabricated by sol-gel method // J Mater Sci: Mater Electron.– 2008.– 19.– P. 1184–1190.
11. **Sze S.M., Kwok K. Ng.** Physics of Semiconductor Devices.- John Wiley & Sons, Inc. 2007.– 816 p.
12. **Brennan K.F., Brown A.S.** Theory of Modern Electronic Semiconductor Devices.- John Wiley & Sons, Inc., 2002.– 448 p.
13. **Yuan L., Cooper J.A., Webb K.J., Melloch M.R.** Demonstration of IMPATT Diode Oscillators in 4H-SiC // Material Science Forum.– 2002.– P. 1359-1362.

14. Characteristics of metal-silicon carbide TUNNEL contact / **V.V. Buniatyan, V.M. Aroutiounian, P.G. Soukiassian, et al** // J. Phys. 4.- France, 2006.– N132.– P. 137-139.
15. **Aroutiounian V.M., Buniatyan V.V., Soukiassian P.** Microwave Characteristics of BARITT Diodes Based on Silicon Carbide // IEEE Trans. Electron Devices.– 1999.– Vol. 46 (3).– P. 585-588.
16. **Robertson J.** Energy levels of point defects in SrTiO<sub>3</sub> and related oxides // J. Appl. Phys.– 2003.– Vol. 93, N2.– P. 1054-1059.
17. **Maier J., Jamnik J., Leonhardt M.** Kinetics of oxygen stoichiometry changes // Solid State Ionics.- 2000.- 129.– P. 25- 32.
18. Oxygen vacancy affect on ferroelectric characteristics (Part 1) / **V.V. Buniatyan, N.W. Martirosyan, V.K. Begoyan, et al** // Proceed. of Engineering Academy of Armenia.– 2011.– Vol. 8, N2.-P. 375–381 and Vol. 8, N3.-P. 542–549.
19. Oxygen vacancy affect on ferroelectric characteristics (Part 2) / **V.V. Buniatyan, N.W. Martirosyan, V.K. Begoyan, et al** // Proceed. of Engineering Academy of Armenia.– 2011.– Vol. 8, N3.-P. 542–549.
20. Dielectric model of point charge defects in insulating paraelectric perovskites / **V.V. Buniatyan, N.W. Martirosyan, A. Vorobiev, et al** // Journal of Applied Physics.– 2011.– 110.– P. 094110-1-11.

National Polytechnic University of Armenia (NPUA). The material is received 02.02.2016.

## Հ.Ռ. ԴԱՇՏՈՅԱՆ

### ՄԻԿՐՈՍԻՏԻՆԱԿԱՆ ԲԻՏՈՒՆԱՆԻ ԳԵՆԵՐԱՑՈՒՄԸ ՄԵՏԱՂ-ՖԵՐՈԷԼԵԿՏՐԻԿ-ՄԵՏԱՂ ՆԱՆՈՎԿԱՌՈՒՑՎԱԾՔՈՒՄ

Առաջին անգամ ուսումնասիրվել են մետաղ-ֆերոէլեկտրիկ-մետաղ կառուցվածքի միկրոալիքային (դինամիկ) բնութագրերը: Ցույց է տրվել, որ այդ կառուցվածքում հնարավոր է ստանալ դինամիկ բացասական դիմադրություն և այդպիսով՝ միկրոալիքային ազդանշանի գեներացիա (ուժեղացում): Ֆերոթաղանթներում, թթվածնի վականսիաներով պայմանավորված, թակարդային մակարդակների կոնցենտրացիայի աճի հետ մեկտեղ աճում են էլքի հզորությունը և սարքի արդյունավետությունը: Հիմնվելով ստացված արդյունքների վրա և համակցելով ֆերոթաղանթային պասսիվ տարրերը, կարելի է նախագծել լիովին ինտեգրված Ferro-VLSI սխեմաներ:

*Առանցքային բառեր*: մետաղ-ֆերոէլեկտրիկ-մետաղ նանոկառուցվածք, դինամիկ բնութագրեր, Ferro-VLSI սխեմա:

## Օ.Ր. ДАШТОЯН

### ГЕНЕРАЦИЯ МИКРОВОЛНОВЫХ СИГНАЛОВ НА НАНОСТРУКТУРЕ МЕТАЛЛ-ФЕРРОЭЛЕКТРИК-МЕТАЛЛ

Исследованы микроволновые (динамические) характеристики структуры металл-ферроэлектрик-металл. Показано, что: в упомянутых структурах возможны получение динамического негативного сопротивления и генерация (усиление) микроволнового сигнала; в ферропленке вместе с ростом концентрации ловушечных уровней, которые обусловлены кислородными вакансиями, растет также мощность выхода и эффективность; на основе полученных результатов и совмещением с пассивными ферропленочными элементами возможно создание полностью интегрированных Ferro-VLSI схем.

*Ключевые слова*: наноструктура металл-ферроэлектрик-металл, динамические характеристики, схема Ferro-VLSI.